Control Engineering Practice 153 (2024) 106090

Contents lists available at ScienceDirect

Control Engineering Practice

journal homepage: www.elsevier.com/locate/conengprac

Robust adaptive PID control of functional electrical stimulation for drop-foot correction

Ghazal Tanhaei [a,*], Hamed Habibi [b], William Holderbaum [c], Noureddin Nakhostin Ansari [a,d,e]

[a] Sports Medicine Research Center, Neuroscience Institute, Tehran University of Medical Sciences, Tehran, Iran
[b] Automation and Robotics Research Group, Interdisciplinary Centre for Security, Reliability and Trust, University of Luxembourg, Luxembourg
[c] School of Biological Sciences, Biomedical Engineering, University of Reading, Reading, United Kingdom
[d] Research Center for War-affected People, Tehran University of Medical Sciences, Tehran, Iran
[e] Department of Physiotherapy, School of Rehabilitation, Tehran University of Medical Sciences, Tehran, Iran

ARTICLE INFO

Keywords:
Adaptive PID control
Self-tuning gain
Functional electrical stimulation
Drop-foot
Muscle fatigue

ABSTRACT

A robust, adaptive proportional–integral–derivative (PID) control strategy is presented for controlling ankle movement using a functional electrical stimulation (FES) neuroprosthesis. The presented control strategy leverages the structurally simple PID controller. Moreover, the proposed PID controller automatically tunes its gains without requiring prior knowledge of the musculoskeletal system. Thus, in contrast to previously proposed control strategies for FES, the proposed controller does not necessitate time-consuming model identification for each patient. Additionally, the computational cost of the controller is minimized by linking the PID gains and updating only the common gain. As a result, a model-free, structurally simple, and computationally inexpensive controller is achieved, making it suitable for wearable FES-based neuroprostheses. A Lyapunov stability analysis proves uniformly ultimately bounded (UUB) tracking of the joint angle. Results from the simulated and experimental trials indicate that the proposed PID controller demonstrates high tracking accuracy and fast convergence.

1. Introduction

Stroke is one of the leading causes of mortality and disability worldwide, with more than 13 million first-time incidents occurring annually (Johnson et al., 2019). Drop-foot manifests in approximately 2 million stroke survivors each year (Johnson, Burridge, Strike, Wood, & Swain, 2004). In addition to stroke, multiple sclerosis (MS), cerebral palsy, spinal cord injury, and traumatic brain injury can also lead to drop-foot (Melo, Silva, Martins, & Newman, 2015). Drop-foot is the paralysis or weakness of the dorsiflexor muscles, which prevents patients from lifting their toes off the ground during the swing phase of gait. Individuals affected by drop-foot often adopt steppage gait or hip hiking as compensatory mechanisms (Błażkiewicz, Wiszomirska, Kaczmarczyk, Brzuszkiewicz-Kuźmicka, & Wit, 2017; Don et al., 2007).

Functional electrical stimulation (FES) is a technique that restores motor function in individuals with central nervous system disorders. In this technique, short electrical pulses are used to generate contractions in paralyzed muscles. These contractions generate torque around the joint associated with the stimulated muscles. The joint's angle can be controlled by modulating the intensity of the electrical stimulation. To actuate the joint in opposite directions, stimulation should be applied to both the flexor and extensor muscles (Lynch & Popovic, 2008). Therefore, applying electrical stimulation to the common peroneal nerve, which innervates the tibialis anterior muscle, can correct drop-foot (Lyons, Sinkjær, Burridge, & Wilcox, 2002). Studies conducted to determine the effectiveness of FES for drop-foot treatment have shown that FES increases walking speed, reduces the effort required for walking and the incidence of falls, and improves quality of life (Barrett & Taylor, 2010; Esnouf, Taylor, Mann, & Barrett, 2010; Roche, Laighin, & Coote, 2009). Furthermore, FES is a long-term, cost-effective treatment for drop-foot (Taylor, Humphreys, & Swain, 2013).

In voluntary contractions, motor units are recruited in order from smallest to largest (Henneman, Somjen, & Carpenter, 1965). However, during transcutaneous electrical stimulation, the recruitment order of motor units is reversed (Feiereisen, Duchateau, & Hainaut, 1997). Thus, in voluntary contraction, slow-twitch, high fatigue-resistant muscle fibers are activated first, whereas during FES, fast-twitch, low fatigue-resistant muscle fibers are activated first (Radák, 2018). Consequently, FES-induced contractions lead to the rapid onset of muscle fatigue.

* Corresponding author.
E-mail addresses: ghazaltanhaei22@gmail.com (G. Tanhaei), hamed.habibi@uni.lu (H. Habibi), w.holderbaum@reading.ac.uk (W. Holderbaum), nakhostin@tums.ac.ir (N.N. Ansari).

https://doi.org/10.1016/j.conengprac.2024.106090
Received 25 April 2024; Received in revised form 23 July 2024; Accepted 5 September 2024
Available online 4 October 2024

After the onset of muscle fatigue, the muscle progressively loses its ability to generate force (Lynch & Popovic, 2008).

All commercially available FES systems for correcting drop-foot use open-loop controllers. In these systems, a trapezoidal envelope is used to adjust the intensity of electrical stimulation during the swing phase of gait. While the trapezoidal envelope guarantees sufficient dorsiflexion during the swing phase, it applies a higher stimulation intensity than required. The inefficiency of the open-loop controller accelerates the onset of muscle fatigue (Melo et al., 2015). In contrast, a closed-loop control system can delay the onset of fatigue by applying just enough stimulation intensity for dorsiflexion during the swing phase.

Over the past two decades, various closed-loop control strategies have been proposed for FES. Sliding mode control (SMC) was used to compensate for uncertainties in the musculoskeletal system, with the nonlinear dynamics modeled by a fuzzy logic system to suppress SMC chattering (Kobravi & Erfanian, 2009). Nonlinear model predictive control (NMPC) was applied to minimize stimulation intensity in two studies (Benoussaad, Mombaur, & Azevedo-Coste, 2013; Kirsch, Alibeji, & Sharma, 2017). Iterative learning control (ILC) was employed to compensate for the time-varying response of muscles to FES (Seel, Werner, Raisch, & Schauer, 2016). Another study suggested the use of repetitive control (RC) to track the cyclic ankle trajectory during gait (Page & Freeman, 2020). While these controllers achieved their design objectives, they all required model identification. Since the dynamics of the musculoskeletal system are time-varying, model identification must be repeated each time a patient uses the neuroprosthesis. The setup time of model-based controllers discourages patients from using the neuroprosthesis.

In a study by Wang, Sharma, Johnson, Gregory, and Dixon (2013), an adaptive inverse optimal controller (IOC) was developed to offer a trade-off between tracking performance and stimulation intensity. The optimal controller was achieved by combining a proportional–derivative (PD) controller with a feedforward neural network (NN). The NN compensated for uncertainties by learning the system dynamics, allowing the proposed controller to bypass the model identification process. However, NN-based controllers required significant computational resources, which shortened the battery life of the wearable neuroprosthesis. In a study by Paz, Oliveira, Pino, and Fontana (2019), an adaptive proportional–integral–derivative (PID) controller was proposed. Extremum seeking control (ESC) was employed to update the PID gains in real-time. However, this approach required manual gain correction to maintain stability, which negatively impacted tracking performance and lacked analytical stability guarantees. Moreover, experimental results showed extremely high fluctuations in the joint angle during the first three cycles (Oliveira, Costa, & Pino, 2016). Hence, the automatic tuning of PID parameters using ESC raised safety concerns. In Oliveira et al. (2017), a combination of SMC and proportional–integral (PI) control was proposed, but despite its integral action, it exhibited significant chattering. While the tuning procedure was simplified, gain optimization still required consideration of both uncertainty bounds and the desired trajectory.

Recent research has explored advanced optimization techniques for tuning PID controllers in FES systems. A study by Ekinci, Izci, Al Nasar, Abu Zitar, and Abualigah (2022) proposed the logarithmic spiral arithmetic optimization algorithm (AOA), while Izci, Ekinci, Eker and Abualigah (2022) introduced a modified opposition-based learning AOA to improve PID tuning. Additionally, Izci, Ekinci, Eker and Demirören (2022) developed a multi-strategy-based weighted mean of vectors algorithm, which was used to design a PID-F controller (PID with a filter for noise reduction). Similarly, Izci, Ekinci, Eker, and Demirören (2023) presented a multi-criteria-based weighted mean of vectors algorithm for enhanced PID tuning. These studies highlight the ongoing interest in developing optimal methods for PID-based FES control.

A dynamic surface controller with delay compensation (DSC-DC), incorporating both ultrasound and kinematic feedback, was proposed by Zhang, Lambeth, Iyer, Sun, and Sharma (2022). This approach improved trajectory tracking and disturbance rejection compared to traditional controllers that used only kinematic feedback. Both Singh and Sharma (2023) and Hodgins and Freeman (2023) explored Model Predictive Control (MPC) schemes for drop foot correction using FES. Singh and Sharma (2023) leveraged a Koopman operator-based framework for system identification, while Hodgins and Freeman (2023) combined FES with pneumatic artificial muscles (PAMs) to reduce fatigue and employed a hybrid MPC controller to optimize gait cycle tracking, minimize fatigue, and manage pressure demands. Although both approaches demonstrated promising results, they relied on computationally intensive model identification and real-time optimization, which limited their practicality for diverse patients. In Jung, Huo, Moon, Amirat, and Mohammed (2021), a hybrid AAFO-FES system (where AAFO stands for actuated ankle–foot orthosis) was employed for foot drop assistance, incorporating a gait-phase-based control strategy for optimized support. While this approach improved ankle trajectory tracking and reduced stimulation intensity, it did not explicitly address stability and relied on anthropometric data for parameter tuning.

In this paper, a robust adaptive PID control method is presented. The controller is designed for a nonlinear musculoskeletal system based on the concept of a core function (CF) (Song, Huang, & Wen, 2015). The core function contains deep-rooted information about the system but is independent of its parameters. Using the core function, uncertainties in the system are compensated without requiring linearization or system modeling. Thus, the CF-based PID controller does not need a model identification process prior to each use. Additionally, by linking the PID gains and carefully selecting a Lyapunov function, a computationally efficient control strategy is achieved. Furthermore, the CF-based PID controller adapts to the time-varying response of muscles to FES-induced fatigue through self-tuning. The main contributions of this paper are as follows:

- Unlike Paz et al. (2019), which uses a manual correction method with limited tracking performance, our approach proposes an automatic PID gain adaptation law that ensures closed-loop system stability without the need for manual correction.
- Unlike Oliveira et al. (2017), our controller does not require knowledge of disturbance bounds or desired trajectories.
- More importantly, our control input is analytically proven and experimentally validated to be continuous and smooth, ensuring patient safety.
- Unlike Ekinci et al. (2022), Izci, Ekinci, Eker and Abualigah (2022), Izci, Ekinci, Eker and Demirören (2022), Izci et al. (2023), which require online optimization, our approach provides closed-form adaptive laws for controller gains, resulting in a computationally efficient method.
- We analytically prove the stability and convergence of our approach for a model with unknown parameters, a feature not present in the aforementioned studies.
- While Zhang et al. (2022) achieved a uniformly ultimately bounded (UUB) tracking error with their DSC-DC controller, our proposed PID-like approach offers advantages in design simplicity and less restrictive gain requirements, making it more practical for real-world implementation.

The rest of the paper is organized as follows: Section 2 presents the problem formulation and technical preliminaries, including the model of ankle dynamics. Section 3 discusses the development of the CF-based PID controller. The Lyapunov stability analysis is provided in Section 4, followed by simulation results in Section 5 and experimental results in Section 6. A detailed discussion on the performance of the CF-based PID controller is presented in Section 7, and finally, conclusions are drawn in Section 8.

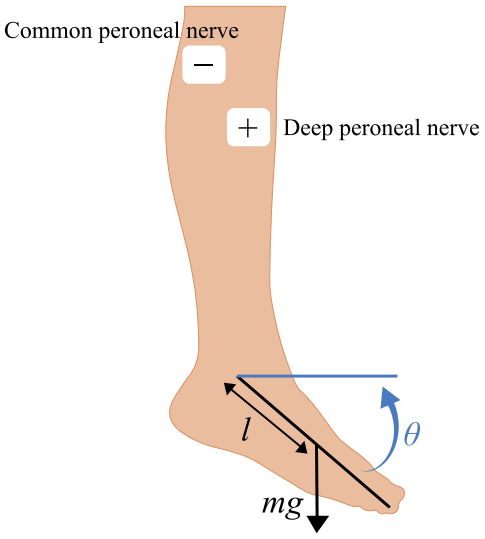

Fig. 1. Schematic diagram of the lower limb showing electrical stimulation of the peroneal nerve. The dorsiflexion angle (θ) is the angle between the foot and the horizontal reference line, which represents 0°. m is the mass of the foot, g is the gravitational acceleration, and l is the distance between the ankle joint and the foot's center of mass.

2. Problem formulation and technical preliminaries

The electrical stimulation of the tibialis anterior muscle is illustrated in Fig. 1. Positive and negative electrodes are placed on the deep peroneal nerve and the common peroneal nerve respectively.

The total applied torque on the ankle is Ferrarin and Pedotti (2000):

$$M_{net}(t) = M_g(t) + M_s(t) + M_d(t) + M_a(t) + d_1(t) \tag{1}$$

where M_g, M_s, and M_d represent gravitational, stiffness, and damping torques, respectively, and d_1 represents system uncertainties. These uncertainties include parameter variations, disturbances, and unmodeled dynamics (e.g., nonlinear torque–angle and torque–velocity scaling factors of the activation dynamics, muscle fatigue). These torques are passive components of the net torque, M_{net}. M_a represents the active ankle torque generated by electrical stimulation. These torques can be modeled as Ferrarin, Palazzo, Riener, and Quintern (2001), Ferrarin and Pedotti (2000):

$$M_g(t) = -mgl \sin\theta(t) \tag{2}$$

$$M_s(t) = -\zeta\,(\theta(t) - \omega)\,\exp(-\varepsilon\,\theta(t)) \tag{3}$$

$$M_d(t) = -\beta\,\dot{\theta}(t) \tag{4}$$

$$M_a(t) = \begin{cases} 0 & 0 \le PW \le PW_{th} \\ \dfrac{S(PW(t) - PW_{th})}{(PW_{sat} - PW_{th})} & PW_{th} < PW < PW_{sat} \\ S & PW_{sat} \le PW \end{cases} \tag{5}$$

Here, m represents the mass of the foot, g is the gravitational acceleration, l is the distance between the ankle joint and the foot's center of mass, and θ denotes the angle between the foot and the horizontal reference line (which represents 0°). ζ and ε are elastic coefficients, ω represents the resting elastic ankle angle (the angle between the shank and foot where the elastic component of the ankle torque is zero), and β is the viscous coefficient. $\dot{\theta}$ represents the ankle angular velocity. Finally, PW denotes the pulse width of electrical stimulation, PW_{th} is the threshold pulse width, PW_{sat} is the saturation pulse width, and S represents the muscle strength.

Considering Dynamics (1), following assumptions are made.

Assumption 1. The desired trajectory (θ_d) and its first and second derivatives ($\dot{\theta}_d$ and $\ddot{\theta}_d$) are known and bounded. Also, $|\ddot{\theta}_d| \le \bar{\theta} < \infty$ where $\bar{\theta}$ is an unknown positive constant.

Assumption 2. The joint angular position and velocity, i.e. θ and $\dot{\theta}$, are measured; therefore, they are known.

Assumption 3. The lumped uncertainty is bounded, i.e. $|d(\theta,t)| \le \bar{d}_1$ where $\bar{d}_1$ is an unknown positive constant.

Assumption 4. Let $f(\theta,t) = (M_g + M_s + M_d)/J$, where J is inertial moment of foot. Considering the system nonlinearities, there exist an unknown constant $w_f \ge 0$, and a computable scalar function $Q_f(\theta,t) \ge 0$ such that $|f(\theta,t)| \le w_f Q_f(\theta,t)$, where the function $Q_f(\theta,t)$ is defined by extracting the deep-rooted information of the system. This function is presented in the control development section.

Remark 1. Assumption 1 can be made since the normal ankle trajectory is available in the literature on gait analysis (Jacquelin Perry, 2010). Assumption 2 is based on the fact that θ can be measured by a sensor that is placed on the foot. Assumption 3 is made based on the results of the experimental trials that were conducted to validate the dynamic model (Ferrarin et al., 2001; Ferrarin & Pedotti, 2000). Assumption 4 is proven to be correct for any practical system with only crude model information (Song et al., 2015).

Following definitions and lemmas are used to design the controller and prove its stability.

Definition 1. Function $N(\chi)$ is called a Nussbaum-type function if $\lim_{s\to\infty} \sup \int_{s_0}^{s} N(\chi)\,\mathrm{d}\chi = +\infty$ and $\lim_{s\to\infty} \inf \int_{s_0}^{s} N(\chi)\,\mathrm{d}\chi = -\infty$ (Song, Huang, & Wen, 2017).

Lemma 1. *Consider the asymmetric non-smooth saturation*

$$H(u(t)) = \begin{cases} 0 & 0 \le u(t) \le m_1 \\ \alpha\,(u(t) - m_1) & m_1 < u(t) < m_2 \\ \bar{u} & m_2 \le u(t) \end{cases} \tag{6}$$

where $\alpha \ge 0$ is the constant slope, m_1 and m_2 are the break points, and $\bar{u}$ is the constant bound of the input $u(t)$. In practice the slope is $\alpha = \bar{u}/(m_2 - m_1)$ to avoid a sudden jump at the break point m_2. Considering the transformation $u'(t) = u - \bar{u}/(2\alpha) - m_1$ and defining

$$G(u'(t)) = \frac{\bar{u}}{2}\left(\frac{e^{\eta u'(t)} - e^{-\eta u'(t)}}{e^{\eta u'(t)} + e^{-\eta u'(t)}}\right) \tag{7}$$

where $\eta > 0$ is a design constant, then it is readily shown that

$$H(u(t)) = G(u'(t)) + D_1(u'(t)) + \frac{\bar{u}}{2} \tag{8}$$

$D_1(u'(t))$ is bounded as $|D_1(u'(t))| \le \bar{D}_1$, where $\bar{D}_1$ is an unknown positive constant. Also, $G(u'(t))$ is differentiable and always in the range $[-\bar{u}/2, \bar{u}/2]$, for all $u(t) \in \mathbb{R}$. By using the mean value theorem, it is easy to show

$$G(u'(t)) = G(u'_0) + \left.\frac{\partial G}{\partial u'}\right|_{u^*} (u'(t) - u'_0) \tag{9}$$

where $u^* = \xi u' + (1-\xi)u'_0$ for $\xi \in (0,1)$. Considering $G(0) = 0$ for $u'_0 = 0$, one can obtain

$$G(u'(t)) = G^* u'(t) \tag{10}$$

where $G^* = \left.\frac{\partial G}{\partial u'}\right|_{\xi u'}$. Also, for all $u(t) \in \mathbb{R}$, G^* is bounded as $|G^*| \le \bar{G}$, where $\bar{G}$ is an unknown positive constant. Accordingly, it can be shown that

$$H(u(t)) = G^*(u(t)) + D(\cdot) \tag{11}$$

where $D(\cdot) = -G^*\bar{u}/(2\alpha) - G^* m_1 + D_1(u'(t)) + \bar{u}/2$ is an unknown bounded variable as $|D(\cdot)| \le \bar{D}$, and $\bar{D} = \bar{G}\bar{u}/(2\alpha) + \bar{G}m_1 + \bar{D}_1 + \bar{u}/2$ is an unknown positive constant.

Remark 2. Inspired by Zhao, Song, and Wen (2016), Lemma 1 approximates the asymmetric non-smooth saturation function by a smooth function. This approximation, owing to its boundedness and smoothness, results in a bounded error. Furthermore, using the mean value theorem, the nonaffine function $H(u(t))$ can be represented as an affine function of its input with an unknown but bounded gain G^*. In the development of the proposed control, this unknown control gain is handled by incorporating a Nussbaum function, as defined in Definition 1.

Lemma 2. *Let $v(t) > 0$ and $\chi(t)$ be smooth functions defined on $[0, t_f)$. For any $t \in [0, t_f)$, if*

$$v(t) < a_0 + e^{-at} \int_0^t (Y(\tau)N(\chi) + 1)\, \dot{\chi} e^{a\tau} \mathrm{d}\tau \tag{12}$$

where a_0 and a are positive constants, and $Y(\tau)$ is a time-varying parameter, which takes values in the unknown interval $L = [l^-, l^+]$ with $0 \notin L$, then $v(t)$, $\chi(t)$, and $\int_0^t Y(\tau)N(\chi)\, \dot{\chi} e^{a\tau} \mathrm{d}\tau$ are bounded on $[0, t_f)$ (Ge, Hong, & Lee, 2004).

Definition 2. The solution of a system $x(t)$ is uniformly ultimately bounded (UUB) if there exists a number $T(K, x(t_0))$, and a $K > 0$ such that for any compact set S and all $x(t_0) \in S$, $\|x(t)\| \leq K$, for all $t \geq t_0 + T$ (Peng, Tian, Zhang, & Du, 2017).

Considering Lemma 1, with $m_1 = PW_{th}$, $m_2 = PW_{sat}$, $\alpha = S/(PW_{sat} - PW_{th})$, and $\bar{u} = S$ one can obtain that

$$M_a(t) = G^* PW(t) + D(PW(t)) \tag{13}$$

The ankle joint rotational dynamics can be simply modeled as

$$J\ddot{\theta}(t) = M_{net}(t) \tag{14}$$

where J is inertial moment of foot, $\ddot{\theta}$ is angular acceleration of foot. By replacing (1)–(5) and (13) in (14), one can obtain

$$\ddot{\theta} = f(\theta, t) + b(\theta, t)u(t) + d(\theta, t) \tag{15}$$

where $f(\theta, t) = \left(-mgl \sin\theta - \zeta(\theta - \omega)\exp(-\varepsilon\theta) - \beta\dot{\theta}\right)/J$, $b(t) = G^*/J$ is an unknown function, $u(t) = PW(t)$ is the control input, and $d(\cdot) = (d_1(\cdot) + D(PW(t)))/J$.

Considering Assumption 3 and Lemma 1, it is readily shown that $|d(\cdot)| \leq \bar{d}$, where $\bar{d} = (\bar{d}_1 + \bar{D})/J$ is an unknown positive constant.

Considering (15), the objective of this paper is to develop a robust adaptive PID controller that achieves UUB tracking of θ without using $f(\cdot)$, $b(\cdot)$, and $d(\cdot)$.

3. Control development

To design the control signal $PW(t)$, the tracking error and its time derivatives are defined as:

$$e(t) = \theta(t) - \theta_d(t) \tag{16}$$

$$\dot{e}(t) = \dot{\theta}(t) - \dot{\theta}_d(t) \tag{17}$$

$$\ddot{e}(t) = \ddot{\theta}(t) - \ddot{\theta}_d(t) = f(\theta, t) + b(\theta, t)PW(t) + d(\theta, t) - \ddot{\theta}_d(t) \tag{18}$$

where θ_d, $\dot{\theta}_d$, and $\ddot{\theta}_d$ are the desired trajectory, velocity, and acceleration, respectively. To proceed, we define a generalized error as

$$E(t) = 2\lambda e(t) + \lambda^2 \int_0^t e(\tau)\, \mathrm{d}\tau + \delta\dot{e}(t) \tag{19}$$

where $\lambda > 0$ and $0 < \delta < 1$ are design parameters such that the transfer function $\delta s^2 + 2\lambda s + \lambda^2$ is Hurwitz. Note that $E(t)$ is formed by combining proportional, integral, and derivative terms of the tracking error $e(t)$. By taking time derivative of $E(t)$, one can obtain:

$$\dot{E} = \delta\ddot{e} + 2\lambda\dot{e} + \lambda^2 e = \delta\left(f(\theta, t) + b(\theta, t)PW + d(\theta, t) - \ddot{\theta}_d\right) + 2\lambda\dot{e} + \lambda^2 e \tag{20}$$

Thus,

$$\dot{E} = F(\theta, t) + B(\theta, t)PW \tag{21}$$

where $F(\theta, t) = \delta f(\theta, t) + \delta d(\theta, t) - \delta\ddot{\theta}_d + 2\lambda\dot{e} + \lambda^2 e$ and $B(\theta, t) = \delta b(\theta, t)$.

Considering Assumptions 1–4, $F(\theta, t)$ is upper bounded as:

$$|F(\theta, t)| \leq \delta w_f Q_f(\theta, t) + \delta\bar{d} + \delta\bar{\theta} + 2\lambda|\dot{e}| + \lambda^2|e| \leq wQ(\theta, t) \tag{22}$$

where $w > 0$ is an unknown constant, and $Q(\theta, t)$ is the "core function" which is an easily computable scalar function (Song et al., 2015).

$$w = \max\left\{\delta w_f, \delta\bar{d}, \delta\bar{\theta}, 2\lambda, \lambda^2\right\} \tag{23}$$

$$Q = Q_f + |\dot{e}| + |e| + 2 \tag{24}$$

For a bounded θ ($-23° \leq \theta \leq 6°$ during the swing phase (Jacquelin Perry, 2010)) and the unknown constant $\varepsilon \in \mathbb{R}$, it is readily shown that $\exp(-\varepsilon\theta) \leq Y$, where Y is an unknown positive constant. Then, considering Assumption 4, $f(\theta, t)$ as in (15), and unknown positive constants m, l, J, ζ, ω, β, it can be shown that

$$w_f = \max\left\{\frac{mgl}{J}, \frac{\zeta Y}{J}, \frac{\zeta\omega Y}{J}, \frac{\beta}{J}\right\} \tag{25}$$

$$Q_f = |\sin\theta| + |\theta| + |\dot{\theta}| + 1 \tag{26}$$

Thus, the core function of the ankle joint dynamics is

$$Q = |\sin\theta| + |\theta| + |\dot{\theta}| + |\dot{e}| + |e| + 3 \tag{27}$$

It can be proven that the boundedness of E guarantees boundedness of e, $\int_0^t e(\tau)\, \mathrm{d}\tau$, and $\dot{e}$ (Khalil, 2000). Thus, the controller is designed to ensure E is UUB.

The CF-based PID controller is proposed as:

$$PW(t) = (k + \Delta k(t))\, N(\chi)E(t) \tag{28}$$

where k is a positive design parameter, $N(\chi)$ is the Nussbaum type function, and the controller gain Δk is obtained via the following adaptive laws:

$$\Delta k = \hat{w}Q^2 \tag{29}$$

$$\dot{\chi} = (k + \Delta k)E^2 \tag{30}$$

$$\dot{\hat{w}} = -\rho_0\hat{w} + \rho_1 Q^2 E^2 \tag{31}$$

where ρ_0 and ρ_1 are positive design constants, and $\hat{w}$ is the estimation of w.

Remark 3. The proposed controller in (28) is composed of two parts, i.e. $(k + \Delta k(t))\, N(\chi)$ and $E(t)$. As mentioned before, $E(t)$ is a PID-like filter of the tracking error. $(k + \Delta k(t))\, N(\chi)$ automatically and adaptively tune PID gains. Thus, the proposed controller is an adaptive PID-like controller.

Remark 4. Adaptive laws in (30) and (31) are scalar functions. Thus, comparing to previous control strategies that used neural network or fuzzy logic for their adaptive laws (Ajoudani & Erfanian, 2009; Nekoukar & Erfanian, 2012), the proposed controller has the significant advantage of being computationally inexpensive.

Remark 5. Amplification of the sensor noise (i.e. high frequency components in $\theta(t)$ signal) by the derivative term can cause fluctuations in $PW(t)$ and instability. Thus, sensitivity of the derivative term to the sensor noise is reduced by $0 < \delta < 1$ in (19).

4. Stability analysis

Theorem 1. *Considering the ankle joint dynamics (15) and their associated uncertainties, under Assumptions 1–4, the proposed controller (28) with adaptive laws (29)–(31) guarantees the following: (1) the tracking error and all internal signals are UUB, and (2) the control signal PW is continuous and smooth everywhere.*

Proof. Consider the following Lyapunov function

$$V = \frac{1}{2}E^2 + \frac{1}{2\rho_1}\tilde{w}^2 \tag{32}$$

where $\tilde{w}$ represents the estimation error of w, defined as $\tilde{w} = w - \hat{w}$. Substituting (21) in the time derivative of V gives

$$\dot{V} = \dot{E}E - \frac{1}{\rho_1}\dot{\hat{w}}\tilde{w} = F(\cdot)E + B(\cdot)PW(\cdot)E - \frac{1}{\rho_1}\dot{\hat{w}}\tilde{w} \tag{33}$$

Considering (22) and (28), $\dot{V}$ is bounded as

$$\dot{V} \le wQ(\cdot)|E| + B(\cdot)(k + \Delta k(\cdot))N(\chi)E^2 - \frac{1}{\rho_1}\dot{\hat{w}}\tilde{w} \tag{34}$$

Substituting (31) in (34) yields

$$\dot{V} \le wQ(\cdot)|E| + B(\cdot)(k + \Delta k(\cdot))N(\chi)E^2 - \tilde{w}Q^2(\cdot)E^2 + \frac{\rho_0}{\rho_1}\tilde{w}\hat{w} \tag{35}$$

Using the Young's inequality and $(\tilde{w} - w)^2 \ge 0$, we have

$$wQ(\cdot)|E| \le wQ^2(\cdot)E^2 + \frac{w}{4} \tag{36}$$

$$\frac{\rho_0}{\rho_1}\tilde{w}\hat{w} \le \frac{\rho_0}{2\rho_1}w^2 - \frac{\rho_0}{2\rho_1}\tilde{w}^2 \tag{37}$$

Integrating (36) and (37) into (35) yields

$$\dot{V} \le \left(k + \hat{w}Q^2(\cdot)\right)E^2 + B(\cdot)(k + \Delta k(\cdot))N(\chi)E^2 - kE^2 - \frac{\rho_0}{2\rho_1}\tilde{w}^2 + \frac{\rho_0}{2\rho_1}w^2 + \frac{w}{4} \tag{38}$$

Substituting (29) and (30) into (38) yields

$$\dot{V} \le (B(\cdot)N(\chi) + 1)\dot{\chi} + c \tag{39}$$

where $B(\cdot) \ne 0$ and $c = \rho_0 w^2/(2\rho_1) + w/4$. Multiplying (39) by e^{at} with $a > 0$ yields

$$\frac{\mathrm{d}V(t)e^{at}}{\mathrm{d}t} \le B(\cdot)N(\chi)\dot{\chi}e^{at} + \dot{\chi}e^{at} + c\,e^{at} \tag{40}$$

Integrating both sides of (40) over $[0, t]$ yields

$$V(t) \le e^{-at}\int_0^t (B(\tau)N(\chi) + 1)\dot{\chi}e^{a\tau}\,\mathrm{d}\tau + \left(V(0) - \frac{c}{a}\right)e^{-at} + \frac{c}{a} \tag{41}$$

Since $0 < e^{-at} \le 1$, $V(t)$ can be further bounded as

$$V(t) \le a_0 + e^{-at}\int_0^t (B(\tau)N(\chi) + 1)\dot{\chi}e^{a\tau}\,\mathrm{d}\tau \tag{42}$$

where $a_0 = c/a + V(0)$ is a positive constant. Considering Lemma 2, it is concluded from (42) that $V(t)$, $\chi(t)$, and $\int_0^t (B(\tau)N(\chi) + 1)\dot{\chi}e^{a\tau}\,\mathrm{d}\tau$ are bounded on $[0, t_f)$. Considering (32), boundedness of $V(t)$ means boundedness of E and $\tilde{w}$. Since w and $\tilde{w} = w - \hat{w}$ are bounded, $\hat{w}$ is bounded. Substituting (32) in (42) and considering the boundedness of $V(0)$ and $\int_0^t (B(\tau)N(\chi) + 1)\dot{\chi}e^{a\tau}\,\mathrm{d}\tau$, it is concluded that

$$\lim_{t\to\infty}\frac{E^2}{2} \le \frac{c}{a} \tag{43}$$

Thus, $|E|$ converges to the set $A = \left\{ |E| \,\middle|\, |E| \le \sqrt{2c/a} \right\}$ as $t \to \infty$.

Considering (19), the boundedness of E, guarantees boundedness of e, $\int_0^t e(\tau)\mathrm{d}\tau$, and $\dot{e}$ (Khalil, 2000). Considering (16) and (17), the boundedness of e, $\dot{e}$, θ_d, and $\dot{\theta}_d$, leads to the boundedness of θ and $\dot{\theta}$. Thus, considering (27), the core function $Q(\theta, t)$ is bounded. Accordingly, from (29) and (31) it is concluded that Δk and $\dot{\hat{w}}$ are bounded. Therefore, considering (28), (21), and (22), PW and $\dot{E}$ are bounded.

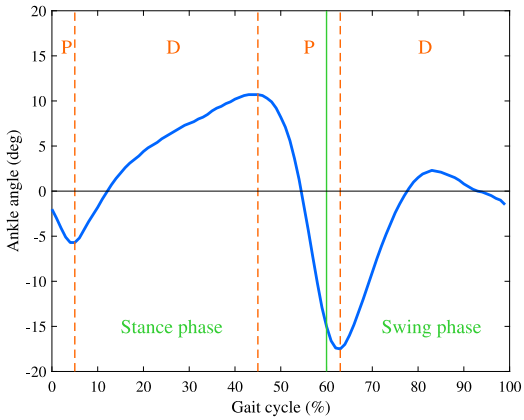

Fig. 2. Sagittal plane ankle angle during a single gait cycle; P and D represent plantar flexion and dorsiflexion, respectively.

Taking the time derivative of Eq. (28), given that $\Delta k = \hat{w}Q^2$ and $N(\chi) = \chi^2\cos(\chi)$, yields

$$\dot{PW} = \frac{\partial PW}{\partial E}\dot{E} + \frac{\partial PW}{\partial N(\chi)}\frac{\partial N(\chi)}{\partial \chi}\dot{\chi} + \frac{\partial PW}{\partial Q}\dot{Q} + \frac{\partial PW}{\partial \hat{w}}\dot{\hat{w}} \tag{44}$$

where

$$\frac{\partial PW}{\partial E} = (k + \Delta k(t))N(\chi) \tag{45}$$

$$\frac{\partial PW}{\partial N(\chi)} = (k + \Delta k(t))E(t) \tag{46}$$

$$\frac{\partial N(\chi)}{\partial \chi} = 2\chi\cos(\chi) - \chi^2\sin(\chi) \tag{47}$$

$$\frac{\partial PW}{\partial Q} = 2\hat{w}QN(\chi)E(t) \tag{48}$$

$$\frac{\partial PW}{\partial \hat{w}} = Q^2N(\chi)E(t) \tag{49}$$

$$\dot{Q} = \frac{\partial Q}{\partial t} = |\dot{\theta}\cos\theta| + |\dot{\theta}| + |\ddot{\theta}| + |\dot{e}| + |\ddot{e}| \tag{50}$$

Since E, $\dot{E}$, $\dot{e}$, $\ddot{e}$, $\dot{\theta}$, $\ddot{\theta}$, Δk, $\hat{w}$, $\dot{\hat{w}}$, χ, $\dot{\chi}$, $N(\chi)$, and Q are all bounded and continuous, $\dot{PW}$ is bounded and continuous. Thus, PW is continuous and smooth everywhere. This ends the proof. □

5. Simulation results

This section presents the results of numerical simulations to evaluate the performance of the CF-based PID controller. The parameters of the controller in (28) were selected as follows: $\lambda = 1$, $\delta = 1$, $k = 0.01$, $\rho_0 = 10$, and $\rho_1 = 0.01$. The even function $N(\chi) = \chi^2\cos(\chi)$ was used in (28) to satisfy Definition 1. Fig. 2 shows the mean values of ankle angles for healthy individuals during a gait cycle (Jacquelin Perry, 2010). The stance phase lasts approximately 60% of the gait cycle, while the swing phase lasts about 40%. Twice during a gait cycle, the ankle undergoes plantarflexion (P) followed by dorsiflexion (D). The first three flexions (P, D, P) occur during the stance phase, and the final dorsiflexion (D) occurs during the swing phase (Jacquelin Perry, 1992). In Fig. 2, the dorsiflexion amplitude during the swing phase is 20°, ranging from −18° to +2°.

The performance of the proposed controller was evaluated using the joint dynamics model presented in section Section 2. The model parameters used in this study were identified for eight male subjects, including five healthy individuals (H1–H5) and three paraplegic patients (P1–P3) (Ferrarin et al., 2001; Ferrarin & Pedotti, 2000). The identification procedure and parameter values are fully described in the cited references. The controller's performance was assessed across different trajectory types: sine wave and ankle (Fig. 2). For the ankle

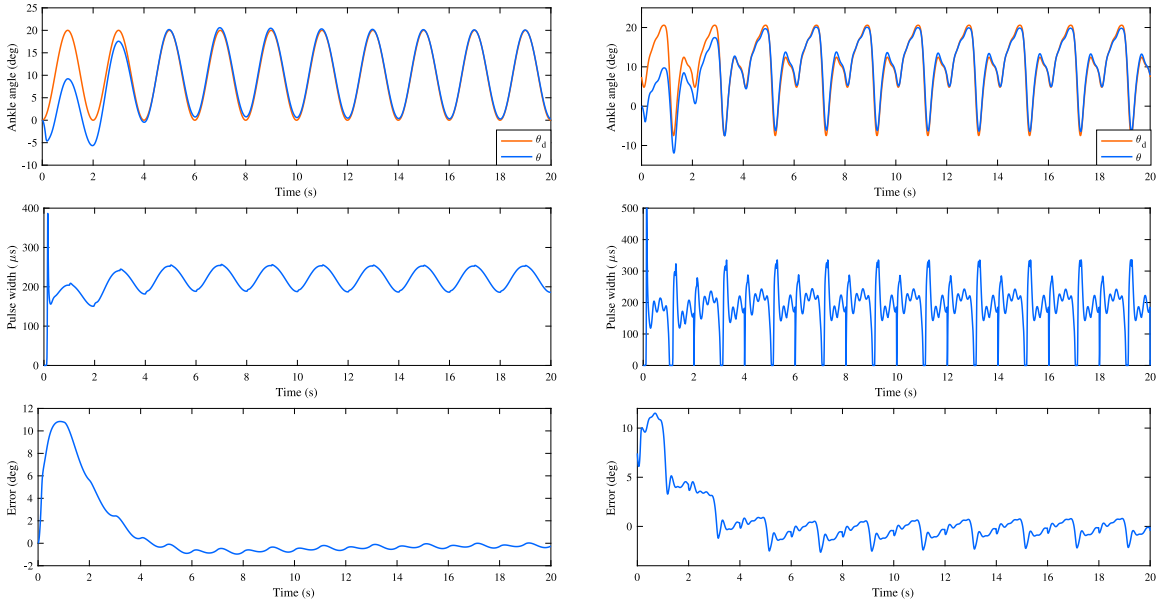

Fig. 3. Controller Performance for Amplitude 20° and Period 2 s: (Left) Sine wave trajectory; (Right) Ankle trajectory. (Top) Desired trajectory (θ_d) and actual trajectory (θ); (Middle) Pulse width; (Bottom) Tracking error.

Table 1
Mean RMS error and standard deviation for different test conditions.

Traj. Type	Amplitude	Period	Mean RMS Error	Std. Dev.
Sine Wave	13°	2 s	2.33°	0.01°
Sine Wave	20°	2 s	2.17°	0.01°
Sine Wave	13°	2.3 s	2.35°	0.01°
Sine Wave	20°	2.3 s	2.19°	0.01°
Ankle Traj.	13°	2 s	2.31°	0.08°
Ankle Traj.	20°	2 s	2.23°	0.20°
Ankle Traj.	13°	2.3 s	2.41°	0.05°
Ankle Traj.	20°	2.3 s	2.20°	0.05°

Table 2
Statistical significance of amplitude and period effects on controller accuracy.

Comparison	p-value	Conclusion
Amplitude Effects		
13° vs. 20° (Sine Wave, 2 s)	1.01×10^{-14}	Significant
13° vs. 20° (Ankle Trajectory, 2 s)	0.43	Not significant
13° vs. 20° (Sine Wave, 2.3 s)	3.80×10^{-17}	Significant
13° vs. 20° (Ankle Trajectory, 2.3 s)	2.07×10^{-6}	Significant
Period Effects		
2 s vs. 2.3 s (Sine Wave, 13°)	3.44×10^{-6}	Significant
2 s vs. 2.3 s (Ankle Trajectory, 13°)	2.83×10^{-5}	Significant
2 s vs. 2.3 s (Sine Wave, 20°)	4.06×10^{-6}	Significant
2 s vs. 2.3 s (Ankle Trajectory, 20°)	0.71	Not significant

trajectory, the amplitude represents the dorsiflexion during the swing phase of gait. The controller was tested at different amplitudes (13° and 20°) and periods (2 s and 2.3 s). These amplitudes and periods were chosen based on previously published studies that measured these values on the paretic side of stroke patients (Von Schroeder, Coutts, Lyden, Billings, & Nickel, 1995; Wang et al., 2020). For each trial, the root mean square (RMS) of the tracking errors (e) during the first 20 s was calculated. Simulations were performed in MATLAB Simulink (MathWorks Inc., USA), with a saturation block used in the Simulink model to bound the control input (PW) between 0 and 500 µs, as $PW < 0$ is unrealistic and $PW > 500$ µs is unsafe for patients.

To illustrate the controller's performance, Fig. 3 presents the results for both a sine wave trajectory and an ankle trajectory, each with an amplitude of 20° and a period of 2 s. The left side of the figure shows the results for the sine wave trajectory, while the right side shows the results for the ankle trajectory. The top row on each side displays the desired trajectory alongside the actual trajectory produced by the controller. The middle row shows the control input (pulse width) that generated this output, and the bottom row presents the tracking error between the desired and actual trajectories. Table 1 summarizes the mean RMS errors and standard deviations for each condition.

Statistical analysis using paired-sample t-tests (Table 2) demonstrated that larger amplitude was associated with a statistically significant reduction in RMS error for sine wave trajectories at both tested periods (2 s and 2.3 s) and for ankle trajectories at a period of 2.3 s. However, no statistically significant difference in RMS error was observed between 13° and 20° for ankle trajectories at a period of 2 s. Additionally, a longer period (2.3 s) resulted in a statistically significant increase in RMS error for sine wave trajectories at both 13° and 20°, as well as for ankle trajectories at 13°. For ankle trajectories at 20°, the period had no statistically significant effect on RMS error.

The observed performance trends might have been influenced by the inherent inaccuracies of the ankle model used in this study. While the model was based on previously published work, it is unlikely that any model can fully capture the complex, non-linear dynamics of the human musculoskeletal system. This inaccuracy could have contributed to the unexpected performance.

To evaluate the controller's ability to adapt to muscle fatigue, the effect of fatigue was simulated by multiplying the muscle activation M_a by the function $-1.5exp(-3t) + 1$. This function gradually reduced the muscle's ability to generate torque over time, mimicking the effects of fatigue. As shown in Fig. 4, after the first two cycles (0–4 s), the controller quickly learned to accurately track the desired trajectory. This adaptation was evident from the control signal (pulse width), which increased by approximately 80 µs from 0–20 s to 240–260 s, effectively compensating for the gradual loss of muscle strength. This adaptive behavior resulted in a significant decrease in the RMS error, from 2.19° in the first 20 s to 0.06° in the last 20 s. This demonstrates the controller's ability to compensate for fatigue and maintain accurate tracking, even under challenging conditions.

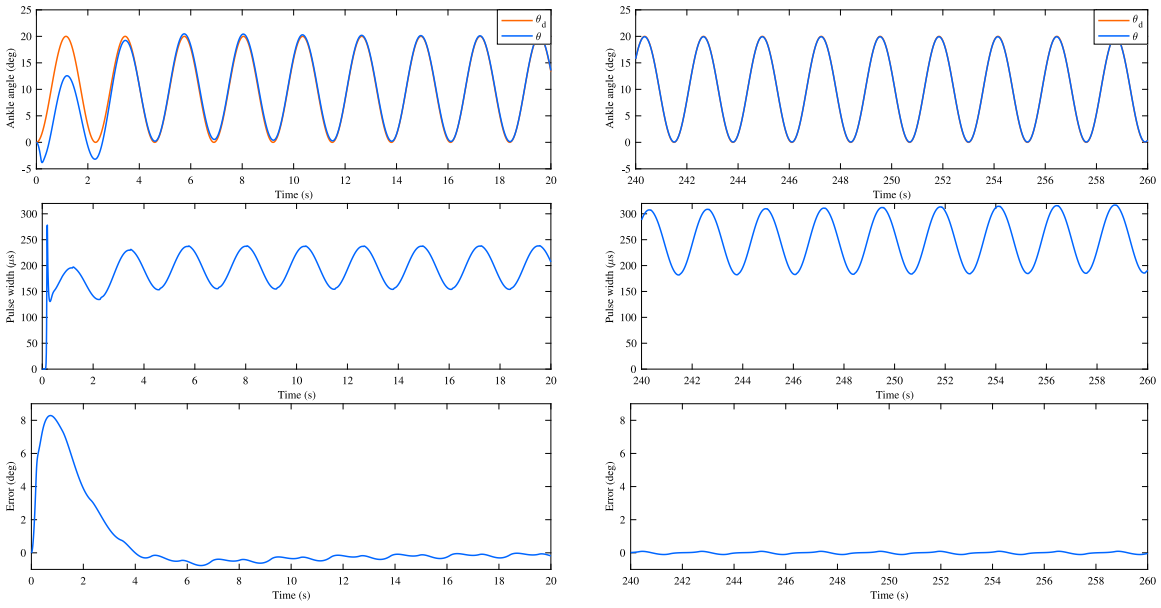

Fig. 4. Controller Performance During Fatigue Simulation: (Left) Tracking from 0–20 s; (Right) Tracking from 240–260 s. (Top) Desired and actual ankle trajectories; (Middle) Pulse width; (Bottom) Tracking error.

6. Experimental results

Following ethical approval[1], experimental trials were conducted on three healthy female subjects aged between 35 and 40 years. Healthy subjects possess intact sensory feedback, allowing for the immediate detection and termination of the experiment if any malfunctioning of the FES system occurred. Each subject sat on a bench with their lower legs hanging over the edge. Self-adhesive electrodes ($5 \times 5\,\text{cm}^2$, axion GmbH, Germany) were placed over the common peroneal nerve and the belly of the tibialis anterior muscle (Fig. 1). A single-channel wearable FES neuroprosthesis was developed to deliver charge-balanced pulses. The CF-based PID controller modulated the pulse width (from 0 to 500 μs) while the current amplitude and frequency were held constant (60 mA and 20 Hz). The parameters of the controller (28) were set to $\lambda = 2$, $\delta = 0.1$, $k = 0.02$, $\rho_0 = 10$, $\rho_1 = 0.01$. The control strategy was programmed on an Arduino Nano microcontroller (www.arduino.cc). A 6-axis inertial measurement unit (MPU-6050, InvenSense Inc., USA) was fixed to the dorsal surface of the foot, over the first metatarsal bone.

Initially, we planned to use force-sensing resistors for gait phase detection during walking trials, with subjects instructed to avoid lifting their feet during the swing phase. However, even with conscious effort, subtle dorsiflexion might occur due to subconscious muscle activation. This ambiguity made it challenging to isolate the effects of the FES system and accurately assess its performance. To address this challenge, we transitioned to a controlled environment. Subjects were seated on a bench, and a pre-recorded ankle trajectory during gait was used. This controlled setup allowed us to isolate and assess the controller's tracking performance during the swing phase, eliminating ambiguity about the origin of movement and enabling controlled FES stimulation. The FES stimulation was applied only during the swing phase of the pre-recorded trajectory, mirroring the practical implementation of a drop foot neuroprosthesis. While this experimental design does not replicate real-world walking, it allowed us to effectively validate the controller's ability to track the desired trajectory in a controlled setting, demonstrating its potential application in drop foot neuroprosthetics.

The controller's performance was evaluated using sine wave and ankle trajectories across a range of amplitudes (13° and 20°) and periods (2 s and 2.3 s), similar to the simulation studies. To illustrate the controller's performance during the experimental trials, Fig. 5 presents representative results for sine wave and ankle trajectories, each with a 20° amplitude and 2 s period. Table 3 summarizes the mean RMS errors and standard deviations for each condition.

Table 3
Mean RMS error and standard deviation for different test conditions.

Traj. Type	Amplitude	Period	Mean RMS Error	Std. Dev.
Sine Wave	13°	2 s	3.38°	0.44°
Sine Wave	20°	2 s	3.61°	0.35°
Sine Wave	13°	2.3 s	3.84°	0.12°
Sine Wave	20°	2.3 s	4.62°	0.22°
Ankle Traj.	13°	2 s	2.84°	0.04°
Ankle Traj.	20°	2 s	2.75°	0.01°
Ankle Traj.	13°	2.3 s	2.71°	0.02°
Ankle Traj.	20°	2.3 s	2.71°	0.02°

Statistical analysis using paired-sample t-tests (Table 4) demonstrated that larger amplitude (20°) was associated with a statistically significant increase in RMS error for sine wave trajectories at a period of 2.3 s, while no significant difference in RMS error was observed between 13° and 20° at a period of 2 s. For ankle trajectories, amplitude did not have a statistically significant effect on RMS error at either period (2 s or 2.3 s). Additionally, a longer period (2.3 s) resulted in a statistically significant increase in RMS error for sine wave trajectories at the larger amplitude of 20°, whereas the increase for 13° was not statistically significant. In contrast, for ankle trajectories, the longer period led to a statistically significant reduction in RMS error at both amplitudes (13° and 20°).

To assess the controller's adaptability in real-world scenarios, an experimental evaluation of muscle fatigue was conducted. The FES system was activated and maintained for a duration of 260 s, allowing for the natural onset of muscle fatigue. As shown in Fig. 6, the controller demonstrated adaptive behavior by increasing the control signal (pulse width) by approximately 100 μs to compensate for the gradual decline in muscle strength. This adaptive response resulted in a significant reduction in the RMS error, from 3.06° at the start of the experiment to 2.05° after 260 s. The experimental results provide further evidence of the controller's ability to compensate for fatigue-induced performance degradation in a practical setting.

[1] IR.TUMS.VCR.REC.1398.114

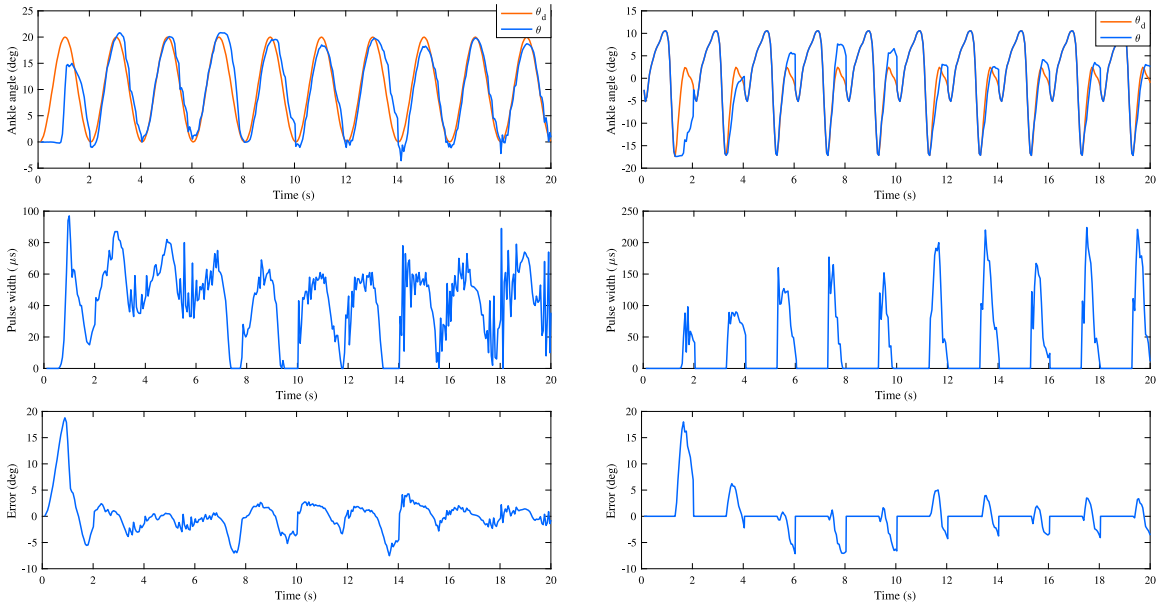

Fig. 5. Controller Performance for Amplitude 20° and Period 2 s: (Left) Sine wave trajectory; (Right) Ankle trajectory. (Top) Desired trajectory (θ_d) and actual trajectory (θ); (Middle) Pulse width; (Bottom) Tracking error.

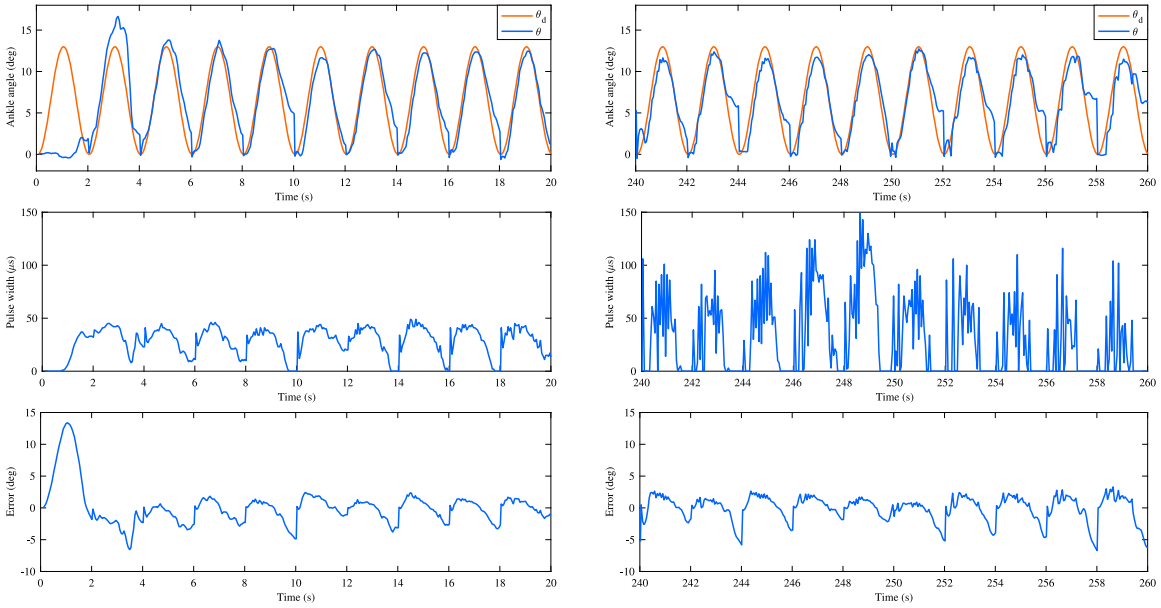

Fig. 6. Controller Performance During Fatigue Experiment: (Left) Tracking from 0–20 s; (Right) Tracking from 240–260 s. (Top) Desired and actual ankle trajectories; (Middle) Pulse width; (Bottom) Tracking error.

Table 4
Statistical significance of amplitude and period effects on controller accuracy.

Comparison	*p*-value	Conclusion
Amplitude Effects		
13° vs. 20° (Sine Wave, 2 s)	0.61	Not significant
13° vs. 20° (Ankle Trajectory, 2 s)	0.08	Not significant
13° vs. 20° (Sine Wave, 2.3 s)	0.03	Significant
13° vs. 20° (Ankle Trajectory, 2.3 s)	0.95	Not significant
Period Effects		
2 s vs. 2.3 s (Sine Wave, 13°)	0.29	Not significant
2 s vs. 2.3 s (Ankle Trajectory, 13°)	0.01	Significant
2 s vs. 2.3 s (Sine Wave, 20°)	0.01	Significant
2 s vs. 2.3 s (Ankle Trajectory, 20°)	0.04	Significant

7. Discussion

The primary limitation of the current study lies in the use of a simulated gait trajectory rather than actual walking during the experimental trials. While this approach allowed for a controlled evaluation of the controller's tracking performance, it does not fully capture the dynamic and complex nature of walking in individuals with neurological impairments. Additionally, the experimental trials were conducted on able-bodied subjects, limiting the generalizability of our findings to patients with drop foot.

Future research is needed to verify the controller's performance in real-world walking scenarios with individuals experiencing drop foot. These trials will involve assessing the controller's effectiveness and safety in more realistic settings, accounting for the unique biomechanical challenges of walking with drop foot. The results of these

future studies will be crucial for advancing the development of FES systems that are both effective and safe for individuals with neurological impairments.

The control input, constrained to 0–500 μs for patient safety, may limit the controller's tracking performance, particularly at larger amplitudes. Future work could explore control strategies that better account for these saturation limits to improve tracking accuracy across a wider range of motions.

The observed RMS error of approximately 3° falls within the range of typical ankle motion for healthy individuals (Jacquelin Perry, 2010). While this suggests that the controller achieves reasonable average tracking accuracy, it is important to acknowledge the potential for overshoot. Overshoot, where the controller transiently exceeds the desired trajectory, can be a significant issue in drop-foot correction applications. It may lead to unnatural movement patterns, hinder gait improvement, and even increase the risk of falls for users.

Future research efforts will focus on mitigating overshoot while maintaining acceptable tracking performance. This could involve fine-tuning the controller parameters or exploring more sophisticated control algorithms specifically designed to minimize overshoot excursions.

The proposed control strategy is applicable to a wide range of electromechanical systems that exhibit second-order dynamics, as defined by Eq. (15) and satisfy Assumptions 1–4. Its inherent robustness to uncertainties and adaptability make it suitable for many electromechanical systems. Our approach has the potential to be extended to diverse applications, including hypersonic vehicle control (Meng, Jiang, & Qi, 2019), attitude control of spacecraft (Van, 2018), wind turbine power control (Habibi, Nohooji, & Howard, 2018), high-speed train control (Guo & Ahn, 2020), and robotic manipulators (Cao & Song, 2020). Further exploration of these applications could lead to significant advancements in various engineering fields.

8. Conclusions

The primary motivation behind developing the CF-based PID controller was to create a computationally efficient control strategy without compromising tracking performance, crucial for real-time implementation in wearable neuroprostheses. By utilizing a core function and linking PID gains, the proposed CF-based PID controller achieves automatic adaptation to individual musculoskeletal systems, eliminates the need for prior model identification, and significantly reduces computational costs. Simulation and experimental results confirm the controller's ability to deliver robust tracking performance for both sinusoidal and ankle trajectories, with effective compensation for muscle fatigue. This research represents a significant advancement in FES control strategies, offering a practical and efficient solution for enhancing mobility in individuals with movement impairments.

CRediT authorship contribution statement

Ghazal Tanhaei: Writing – review & editing, Writing – original draft, Visualization, Validation, Software, Resources, Methodology, Investigation, Funding acquisition, Formal analysis, Data curation, Conceptualization. **Hamed Habibi:** Writing – review & editing, Validation, Methodology. **William Holderbaum:** Validation, Supervision. **Noureddin Nakhostin Ansari:** Supervision, Resources, Project administration, Conceptualization.

Declaration of competing interest

The authors declare that they have no known competing financial interests or personal relationships that could have appeared to influence the work reported in this paper.

Acknowledgments

The authors would like to express their gratitude to the Djavad Mowafaghian Research Center for Intelligent Neuro-Rehabilitation Technologies for their invaluable support and resources, which made this research possible. This work was supported by the Iran's Organization for Development of International Cooperation in Science and Technology.

References

Ajoudani, A., & Erfanian, A. (2009). A neuro-sliding-mode control with adaptive modeling of uncertainty for control of movement in paralyzed limbs using functional electrical stimulation. *IEEE Transactions on Biomedical Engineering*, *56*(7), 1771–1780.

Barrett, C., & Taylor, P. (2010). The effects of the odstock drop foot stimulator on perceived quality of life for people with stroke and multiple sclerosis. *Neuromodulation: Technology at the Neural Interface*, *13*(1), 58–64.

Benoussaad, M., Mombaur, K., & Azevedo-Coste, C. (2013). Nonlinear model predictive control of joint ankle by electrical stimulation for drop foot correction. In *2013 IEEE/RSJ international conference on intelligent robots and systems* (pp. 983–989). IEEE.

Błażkiewicz, M., Wiszomirska, I., Kaczmarczyk, K., Brzuszkiewicz-Kuźmicka, G., & Wit, A. (2017). Mechanisms of compensation in the gait of patients with drop foot. *Clinical Biomechanics*, *42*, 14–19.

Cao, Y., & Song, Y.-D. (2020). Adaptive PID-like fault-tolerant control for robot manipulators with given performance specifications. *International Journal of Control*, *93*(3), 377–386.

Don, R., Serrao, M., Vinci, P., Ranavolo, A., Cacchio, A., Ioppolo, F., et al. (2007). Foot drop and plantar flexion failure determine different gait strategies in charcot-marie-tooth patients. *Clinical Biomechanics*, *22*(8), 905–916.

Ekinci, S., Izci, D., Al Nasar, M. R., Abu Zitar, R., & Abualigah, L. (2022). Logarithmic spiral search based arithmetic optimization algorithm with selective mechanism and its application to functional electrical stimulation system control. *Soft Computing*, *26*(22), 12257–12269.

Esnouf, J., Taylor, P., Mann, G., & Barrett, C. (2010). Impact on activities of daily living using a functional electrical stimulation device to improve dropped foot in people with multiple sclerosis, measured by the Canadian occupational performance measure. *Multiple Sclerosis Journal*, *16*(9), 1141–1147.

Feiereisen, P., Duchateau, J., & Hainaut, K. (1997). Motor unit recruitment order during voluntary and electrically induced contractions in the tibialis anterior. *Experimental Brain Research*, *114*, 117–123.

Ferrarin, M., Palazzo, F., Riener, R., & Quintern, J. (2001). Model-based control of FES-induced single joint movements. *IEEE Transactions on Neural Systems and Rehabilitation Engineering*, *9*(3), 245–257.

Ferrarin, M., & Pedotti, A. (2000). The relationship between electrical stimulus and joint torque: A dynamic model. *IEEE Transactions on Rehabilitation Engineering*, *8*(3), 342–352.

Ge, S. S., Hong, F., & Lee, T. H. (2004). Adaptive neural control of nonlinear time-delay systems with unknown virtual control coefficients. *IEEE Transactions on Systems, Man, and Cybernetics, Part B (Cybernetics)*, *34*(1), 499–516.

Guo, X.-G., & Ahn, C. K. (2020). Adaptive fault-tolerant pseudo-PID sliding-mode control for high-speed train with integral quadratic constraints and actuator saturation. *IEEE Transactions on Intelligent Transportation Systems*, *22*(12), 7421–7431.

Habibi, H., Nohooji, H. R., & Howard, I. (2018). Adaptive PID control of wind turbines for power regulation with unknown control direction and actuator faults. *IEEE Access*, *6*, 37464–37479.

Henneman, E., Somjen, G., & Carpenter, D. O. (1965). Functional significance of cell size in spinal motoneurons. *Journal of Neurophysiology*, *28*(3), 560–580.

Hodgins, L., & Freeman, C. T. (2023). A hybrid orthosis combining functional electrical stimulation and soft robotics for improved assistance of drop-foot. *Medical Engineering & Physics*, *115*, Article 103979.

Izci, D., Ekinci, S., Eker, E., & Abualigah, L. (2022). Opposition-based arithmetic optimization algorithm with varying acceleration coefficient for function optimization and control of fes system. In *Proceedings of international joint conference on advances in computational intelligence: IJCACI 2021* (pp. 283–293). Springer.

Izci, D., Ekinci, S., Eker, E., & Demirören, A. (2022). Multi-strategy modified INFO algorithm: Performance analysis and application to functional electrical stimulation system. *Journal of Computer Science*, *64*, Article 101836.

Izci, D., Ekinci, S., Eker, E., & Demirören, A. (2023). Biomedical application of a random learning and elite opposition-based weighted mean of vectors algorithm with pattern search mechanism. *Journal of Control, Automation and Electrical Systems*, *34*(2), 333–343.

Jacquelin Perry, M. (1992). *Gait analysis: normal and pathological function*. New Jersey: SLACK.

Jacquelin Perry, M. (2010). *Gait analysis: normal and pathological function*. New Jersey: SLACK.

Johnson, C. A., Burridge, J. H., Strike, P. W., Wood, D. E., & Swain, I. D. (2004). The effect of combined use of botulinum toxin type a and functional electric stimulation in the treatment of spastic drop foot after stroke: A preliminary investigation. *Archives of Physical Medicine and Rehabilitation*, *85*(6), 902–909.

Johnson, C. O., Nguyen, M., Roth, G. A., Nichols, E., Alam, T., Abate, D., et al. (2019). Global, regional, and national burden of stroke, 1990–2016: A systematic analysis for the global burden of disease study 2016. *The Lancet Neurology*, *18*(5), 439–458.

Jung, P.-G., Huo, W., Moon, H., Amirat, Y., & Mohammed, S. (2021). A novel gait phase detection algorithm for foot drop correction through optimal hybrid FES-orthosis assistance. In *2021 IEEE international conference on robotics and automation* (pp. 10391–10397). IEEE.

Khalil, H. K. (2000). Universal integral controllers for minimum-phase nonlinear systems. *IEEE Transactions on Automatic Control*, *45*(3), 490–494.

Kirsch, N., Alibeji, N., & Sharma, N. (2017). Nonlinear model predictive control of functional electrical stimulation. *Control Engineering Practice*, *58*, 319–331.

Kobravi, H.-R., & Erfanian, A. (2009). Decentralized adaptive robust control based on sliding mode and nonlinear compensator for the control of ankle movement using functional electrical stimulation of agonist–antagonist muscles. *Journal of Neural Engineering*, *6*(4), Article 046007.

Lynch, C. L., & Popovic, M. R. (2008). Functional electrical stimulation. *IEEE Control Systems Magazine*, *28*(2), 40–50.

Lyons, G. M., Sinkjær, T., Burridge, J. H., & Wilcox, D. J. (2002). A review of portable FES-based neural orthoses for the correction of drop foot. *IEEE Transactions on Neural Systems and Rehabilitation Engineering*, *10*(4), 260–279.

Melo, P., Silva, M., Martins, J., & Newman, D. (2015). Technical developments of functional electrical stimulation to correct drop foot: sensing, actuation and control strategies. *Clinical Biomechanics*, *30*(2), 101–113.

Meng, Y., Jiang, B., & Qi, R. (2019). Adaptive fault-tolerant attitude tracking control of hypersonic vehicle subject to unexpected centroid-shift and state constraints. *Aerospace Science and Technology*, *95*, Article 105515.

Nekoukar, V., & Erfanian, A. (2012). A decentralized modular control framework for robust control of FES-activated walker-assisted paraplegic walking using terminal sliding mode and fuzzy logic control. *IEEE Transactions on Biomedical Engineering*, *59*(10), 2818–2827.

Oliveira, T. R., Costa, L. R., Catunda, J. M. Y., Pino, A. V., Barbosa, W., & de Souza, M. N. (2017). Time-scaling based sliding mode control for neuromuscular electrical stimulation under uncertain relative degrees. *Medical Engineering & Physics*, *44*, 53–62.

Oliveira, T. R., Costa, L. R., & Pino, A. V. (2016). Extremum seeking applied to neuromuscular electrical stimulation. *IFAC-PapersOnLine*, *49*(32), 188–193.

Page, A., & Freeman, C. (2020). Point-to-point repetitive control of functional electrical stimulation for drop-foot. *Control Engineering Practice*, *96*, Article 104280.

Paz, P., Oliveira, T. R., Pino, A. V., & Fontana, A. P. (2019). Model-free neuromuscular electrical stimulation by stochastic extremum seeking. *IEEE Transactions on Control Systems Technology*, *28*(1), 238–253.

Peng, C., Tian, E., Zhang, J., & Du, D. (2017). Decentralized event-triggering communication scheme for large-scale systems under network environments. *Information Sciences*, *380*, 132–144.

Radák, Z. (2018). Chapter 2 - skeletal muscle, function, and muscle fiber types. In Z. Radák (Ed.), *The physiology of physical training* (pp. 15–31). Academic Press, http://dx.doi.org/10.1016/B978-0-12-815137-2.00002-4, URL https://www.sciencedirect.com/science/article/pii/B9780128151372000024.

Roche, A., Laighin, G. ó., & Coote, S. (2009). Surface-applied functional electrical stimulation for orthotic and therapeutic treatment of drop-foot after stroke–A systematic review. *Physical Therapy Reviews*, *14*(2), 63–80.

Seel, T., Werner, C., Raisch, J., & Schauer, T. (2016). Iterative learning control of a drop foot neuroprosthesis—Generating physiological foot motion in paretic gait by automatic feedback control. *Control Engineering Practice*, *48*, 87–97.

Singh, M., & Sharma, N. (2023). Data-driven model predictive control for drop foot correction. In *2023 American control conference* (pp. 2615–2620). IEEE.

Song, Y., Huang, X., & Wen, C. (2015). Tracking control for a class of unknown nonsquare MIMO nonaffine systems: A deep-rooted information based robust adaptive approach. *IEEE Transactions on Automatic Control*, *61*(10), 3227–3233.

Song, Y., Huang, X., & Wen, C. (2017). Robust adaptive fault-tolerant PID control of MIMO nonlinear systems with unknown control direction. *IEEE Transactions on Industrial Electronics*, *64*(6), 4876–4884.

Taylor, P., Humphreys, L., & Swain, I. (2013). The long-term cost-effectiveness of the use of functional electrical stimulation for the correction of dropped foot due to upper motor neuron lesion.. *Journal of Rehabilitation Medicine*, *45*(2), 154–160.

Van, M. (2018). An enhanced robust fault tolerant control based on an adaptive fuzzy PID-nonsingular fast terminal sliding mode control for uncertain nonlinear systems. *IEEE/ASME Transactions on Mechatronics*, *23*(3), 1362–1371.

Von Schroeder, H. P., Coutts, R. D., Lyden, P. D., Billings, E., & Nickel, V. L. (1995). Gait parameters following stroke: A practical assessment. *Journal of Rehabilitation Research and Development*, *32*, 25–31.

Wang, Y., Mukaino, M., Ohtsuka, K., Otaka, Y., Tanikawa, H., Matsuda, F., et al. (2020). Gait characteristics of post-stroke hemiparetic patients with different walking speeds. *International Journal of Rehabilitation Research*, *43*(1), 69–75.

Wang, Q., Sharma, N., Johnson, M., Gregory, C. M., & Dixon, W. E. (2013). Adaptive inverse optimal neuromuscular electrical stimulation. *IEEE Transactions on Cybernetics*, *43*(6), 1710–1718.

Zhang, Q., Lambeth, K., Iyer, A., Sun, Z., & Sharma, N. (2022). Ultrasound imaging-based closed-loop control of functional electrical stimulation for drop foot correction. *IEEE Transactions on Control Systems Technology*, *31*(3), 989–1005.

Zhao, K., Song, Y., & Wen, C. (2016). Computationally inexpensive fault tolerant control of uncertain non-linear systems with non-smooth asymmetric input saturation and undetectable actuation failures. *IET Control Theory & Applications*, *10*(15), 1866–1873.